JCI insight

RESEARCH ARTICLE

Functional correction of dystrophin actin binding domain mutations by genome editing

Viktoriia Kyrychenko,[1,2,3] Sergii Kyrychenko,[1,2,3] Malte Tiburcy,[4,5] John M. Shelton,[6] Chengzu Long,[1,2,3] Jay W. Schneider,[2,3,6] Wolfram-Hubertus Zimmermann,[4,5] Rhonda Bassel-Duby,[1,2,3] and Eric N. Olson[1,2,3]

[1]Department of Molecular Biology, [2]Senator Paul D. Wellstone Muscular Dystrophy Cooperative Research Center, and [3]Hamon Center for Regenerative Science and Medicine, University of Texas Southwestern Medical Center, Dallas, Texas, USA. [4]Institute of Pharmacology and Toxicology, University Medical Center Göttingen, Göttingen, Germany. [5]DZHK (German Center for Cardiovascular Research), Partner Site Göttingen, Göttingen, Germany. [6]Department of Internal Medicine, University of Texas Southwestern Medical Center, Dallas, Texas, USA.

Dystrophin maintains the integrity of striated muscles by linking the actin cytoskeleton with the cell membrane. Duchenne muscular dystrophy (DMD) is caused by mutations in the dystrophin gene (*DMD*) that result in progressive, debilitating muscle weakness, cardiomyopathy, and a shortened lifespan. Mutations of dystrophin that disrupt the amino-terminal actin-binding domain 1 (ABD-1), encoded by exons 2–8, represent the second-most common cause of DMD. In the present study, we compared three different strategies for CRISPR/Cas9 genome editing to correct mutations in the ABD-1 region of the *DMD* gene by deleting exons 3–9, 6–9, or 7–11 in human induced pluripotent stem cells (iPSCs) and by assessing the function of iPSC-derived cardiomyocytes. All three exon deletion strategies enabled the expression of truncated dystrophin protein and restoration of cardiomyocyte contractility and calcium transients to varying degrees. We show that deletion of exons 3–9 by genomic editing provides an especially effective means of correcting disease-causing ABD-1 mutations. These findings represent an important step toward eventual correction of common *DMD* mutations and provide a means of rapidly assessing the expression and function of internally truncated forms of dystrophin-lacking portions of ABD-1.

Introduction

Dystrophin is a large intracellular protein that stabilizes muscle membranes against forces associated with contraction and stretch by providing a mechanical link between the intracellular actin cytoskeleton and the transmembrane dystroglycan complex (1). The *DMD* gene, one of the largest human genes, encodes dystrophin and is composed of 79 exons on the Xp21 chromosome. Mutations that disrupt the open reading frame of dystrophin lead to Duchenne muscular dystrophy (DMD), a life-limiting, rapidly progressive form of muscular dystrophy (2, 3). DMD is an X-linked recessive disorder affecting 1:5,000 boys. Loss of dystrophin destabilizes muscle membranes, allowing excess calcium into cardiac and skeletal muscle cells, resulting in muscle degeneration and necrosis (4, 5). Internal deletion mutations in the dystrophin gene (*DMD*) that preserve the amino- and carboxyl-termini of the protein but eliminate various internal rod domains cause Becker muscular dystrophy (BMD), a relatively mild muscle disease (6).

DMD is associated with greater than 4,000 mutations in the DMD gene (7). These mutations are comprised primarily of exon deletions, as well as exon duplications and small mutations that include point mutations. DMD mutations cluster into two hot-spot regions of the gene (7, 8). One hot spot is located within the 5′ region of the gene, encompassing exons 2–20. These mutations account for approximately 15% of all exon deletions and approximately 50% of all exon duplications within the *DMD* gene. Deletion of exons 3–7 are the most frequent. The second DMD hot spot is located in the distal region of the *DMD* gene, between exons 45–55, accounting for approximately 70% of all exon deletions and approximately 15% of all exon duplications (9, 10).

Conflict of interest: RBD and ENO are consultants for Exonics Therapeutics. WHZ is a cofounder and, together with MT, scientific advisor of Myriamed.

Submitted: June 26, 2017
Accepted: August 15, 2017
Published: September 21, 2017

Reference information:
JCI Insight. 2017;2(18):e95918.
https://doi.org/10.1172/jci.insight.95918.

Dystrophin protein consists of 3,685 amino acids and can be separated into four domains: (i) the actin binding domain 1 (ABD-1), which consists of amino acids 14-240 and connects the filamentous elements of the cytoskeleton to the cell membrane; (ii) the central rod domain, composed of 24 spectrin-like repeats and the second actin-binding domain (ABD-2); (iii) the cysteine-rich domain; and (iv) the carboxyl-terminal domain. Together, these four domains provide the function of dystrophin as a structural link between the cytoskeleton and extracellular matrix to maintain muscle integrity.

The dystrophin protein can tolerate internal deletions that maintain a subset of the rod domains with intact amino- and carboxyl-termini regions, resulting in mild loss of muscle function, as seen in patients with BMD (11). There have been numerous strategies to convert DMD to BMD by skipping or deleting out-of-frame exons and restoring the expression of truncated forms of dystrophin protein (12–17). Similarly, shortened forms of dystrophin, referred to as mini- or microdystrophins, are being developed for gene therapy (18–20). It should be noted that the precise consequences of in-frame deletions on the stability and function of dystrophin are not predictable a priori, as some in-frame deletions cause severe disease while others have only mild effects (10, 21). Thus, it is important to analyze the dystrophin protein products generated from in-frame deletions before reaching conclusions regarding their potential therapeutic effects.

Previously, we and others used CRISPR/Cas9-mediated genome editing to permanently correct dystrophin mutations in mouse models of DMD and patient-derived muscle cells (12–17, 22–25). These efforts focused mainly on correcting mutations in the spectrin-like repeat region to restore dystrophin function by generating truncated dystrophin protein, similar to the forms associated with BMD. The ABD-1 of dystrophin contains three actin-binding sites (ABS1-3) that associate with filamentous actin (F-actin) and are essential for the stabilization of muscle membranes by dystrophin (26–29). Little emphasis has been put on editing the ABD-1 region of the *DMD* gene, although approximately 7% of DMD patients have mutations in the ABD-1 domain. In fact, exons 2–7, which encode part of the ABD-1, are the most frequently mutated portion of the 5′-proximal hot spot (8). Two reports have described genomic editing of a *DMD* mutation comprising a duplication of exon 2 (30, 31), and other reports showed editing of an exon 7 splice site mutation in the golden retriever dog model of DMD (32, 33). In-frame deletions and missense mutations of the 5′ region of the *DMD* gene that affect the ABD-1 structure have been associated with a decrease in dystrophin protein stability, reduced actin binding affinity, and protein mis-folding and degradation (21, 27, 34–36). This raises the possibility that restoring the open reading frame of ABD-1 mutations by genome editing strategies may not be sufficient to correct DMD. Functional assessment of the ABD-1 truncated dystrophin protein should be used to determine restoration of muscle stability. Of note, medical case studies have reported patients with deletions in exons 3–9 in the *DMD* gene that exhibit no apparent phenotype, suggesting that precise deletion of exons 3–9 may be an effective approach to correct mutations in the ABD-1 region (37, 38).

Human induced pluripotent stem cells (iPSCs) offer a unique opportunity for studying human diseases in a dish (39). Their unlimited proliferation and ability to undergo clonal selection and differentiation into different cell types provide a reliable platform for testing gene editing strategies to either create or correct human mutations. Differentiation of DMD-derived iPSCs to cardiomyocytes prior to and following genome editing allows the analysis of DMD phenotypes by assessing dystrophin expression and cardiomyocyte function, such as muscle contractility and Ca^{2+} handling. Assembly of iPSC-derived cardiomyocytes as engineered heart muscle (EHM) allows for direct and controlled measurements of heart muscle force of contraction (40).

Here, we introduced an exon 8–9 deletion (ΔEx8-9) in the *DMD* gene of healthy donor–derived iPSCs to generate a DMD iPSC line. This ΔEx8-9 DMD iPSC line allowed us to correct the DMD mutation by various gene editing strategies and then assess truncated dystrophin functionality in comparison with isogenic control cells. We corrected the ΔEx8-9 mutation using three different exon-deletion strategies to restore the open reading frames: (i) deleting exons 3–7 to generate ΔEx3-9, which excises the ABS-2 and ABS-3 regions; (ii) deleting exons 6–7 to generate ΔEx6-9, which excises ABS-3; and (iii) deleting exons 7–11 to generate ΔEx7-11, which leaves all three ABS regions intact. We show that deletion of *DMD* exons 3–9 generates a truncated dystrophin but maintains the structure of dystrophin such that it restores cardiomyocyte functionality. These findings provide a promising strategy for correction of DMD mutations within the proximal hot spot of the *DMD* gene by genomic editing, allowing restoration of dystrophin expression and function.

Results

Generating a dystrophin mutation that disrupts the ABD-1. We generated a human iPSC line with a deletion of exons 8 and 9 in the *DMD* gene using CRISPR/Cas9-mediated editing to analyze the effect of ABD-1 deletions on muscle function (Figure 1A). Two single guide RNAs (gRNAs), targeting sequences in intron 7 and intron 9 of the *DMD* gene in the presence of *Streptococcus pyogenes* Cas9, were used to delete *DMD* exons 8–9 in healthy human iPSCs (Figure 1B). This induced DMD mutant human cell line is referred to as ΔEx8-9 iDMD, and represents the common 5′-proximal hot-spot mutations. Human iPSCs harboring *DMD* exon 8–9 deletions were picked by clonal selection, and the mutation was confirmed by sequencing genomic DNA (Figure 1C). The human ΔEx8-9 iDMD iPSC line has a 1,909-bp deletion, which generates a newly formed junction between intron 7 to intron 9 (Figure 1C). Primers within intron 7 flanking the gRNA-7 targeting site were used to validate the deletion and, as expected, showed no PCR product with ΔEx8-9 iDMD compared with control iPSC with a 424-bp product (Figure 1C). The ΔEx8-9 iDMD iPSCs were differentiated to cardiomyocytes, and reverse transcription PCR (RT-PCR) was performed using forward and reverse primers targeting exons 1 and 10, respectively (Figure 1D). Sequencing of the RT-PCR products showed splicing of exon 7 to exon 10, which created a premature stop codon following the first 5 amino acids encoded by exon 10 (Figure 1D). Loss of dystrophin protein was confirmed by Western blot analysis and immunocytochemistry in ΔEx8-9 iDMD iPSC–derived cardiomyocytes (Figure 1, E and F).

Correction of the ΔEx8-9 iDMD mutation by exon deletion strategies. Three different CRISPR/Cas9-mediated strategies were used to correct the mutation in ΔEx8-9 iDMD iPSCs in order to restore the dystrophin open reading frame (Figure 2A). These strategies generated dystrophin with different truncations in the ABD-1 domain, providing a means of analyzing the effect of ABD-1 deletions on muscle function. For each strategy, we applied two gRNAs to delete multiple exons and analyzed two independent iPSC clones. Strategy no. 1 generated ΔEx3-9 iPSCs, by targeting intron 2 and intron 7 with gRNAs and deleting exons 3–7 (Figure 2B). Genomic sequencing of the genome edited region showed a hybrid junction of intron 2 to intron 7, confirming generation of ΔEx3-9 iPSCs (Figure 2C). Following differentiation of ΔEx3-9 iPSCs to cardiomyocytes, RT-PCR was performed using primers within exon 1 and exon 10 (Figure 2D). Sequencing of the RT-PCR product showed splicing of exon 2 to exon 10. Restoration of the *DMD* open reading frame generated a truncated dystrophin protein lacking the ABS-2 and ABS-3 regions. Dystrophin expression was confirmed by Western blot analysis and immunocytochemistry of ΔEx3-9 iPSC–derived cardiomyocytes (Figure 2, E and F, and Supplemental Figure 1A; supplemental material available online with this article; https://doi.org/10.1172/jci.insight.95918DS1).

Strategy no. 2 generated ΔEx6-9 iPSCs, using gRNAs targeting intron 5 and intron 7 in order to delete exons 6 and 7 (Figure 3A). This form of CRISPR/Cas9 editing resulted in deletion of exon 6 through exon 9, which was confirmed by sequencing of genomic PCR products (Figure 3B). Following differentiation, RT-PCR using primers within exon 1 and exon 10 was performed on ΔEx6-9 iPSC–derived cardiomyocytes, and sequencing of the RT-PCR product confirmed splicing of exon 5 to exon 10 (Figure 3C). Restoration of dystrophin expression generated a truncated protein lacking the ABS-3 region. Dystrophin expression was confirmed by Western blot analysis and immunocytochemistry in ΔEx6-9 iPSC–derived cardiomyocytes (Figure 3, D and E, and Supplemental Figure 1, A and B).

Strategy no. 3 generated ΔEx7-11 iPSCs, using gRNAs targeting introns 6 and 11 to delete exons 7–11 of ΔEx8-9 iDMD iPSCs (Figure 4A). This genome editing strategy introduced the largest deletion of 164 kb in ΔEx8-9 iDMD iPSCs. Similar to the first two correction strategies, single cell–derived colonies were picked from the corrected iPSC pool, and the genomic region was sequenced to confirm editing (Figure 4B). The ΔEx7-11 iPSCs were differentiated to cardiomyocytes, and RT-PCR was performed with primers within exon 5 and exon 12 to reveal splicing of exon 6 to exon 12, as seen by sequencing (Figure 4C). Restoration of the *DMD* open reading frame of ΔEx7-11 iPSC–derived cardiomyocytes generated a truncated dystrophin protein lacking amino acids 177–444 but with all three ABS intact. Dystrophin expression was confirmed by Western blot analysis and immunocytochemistry (Figure 4, D and E, and Supplemental Figure 1, A and B). We observed less dystrophin expression in ΔEx7-11 iPSC–derived cardiomyocytes compared with control iPSC–derived cardiomyocytes and the other corrected lines, ΔEx3-9 and ΔEx6-9. Previously, it was shown that missense mutations associated with the DMD phenotype caused steady-state decreases in dystrophin protein levels inversely proportional to the tertiary stability and directly caused by proteasomal degradation (41). Consistent with this report, we observed increased dystrophin protein levels when ΔEx7-11 iPSC–derived cardiomyocytes were treated with the proteasome inhibitor MG-132,

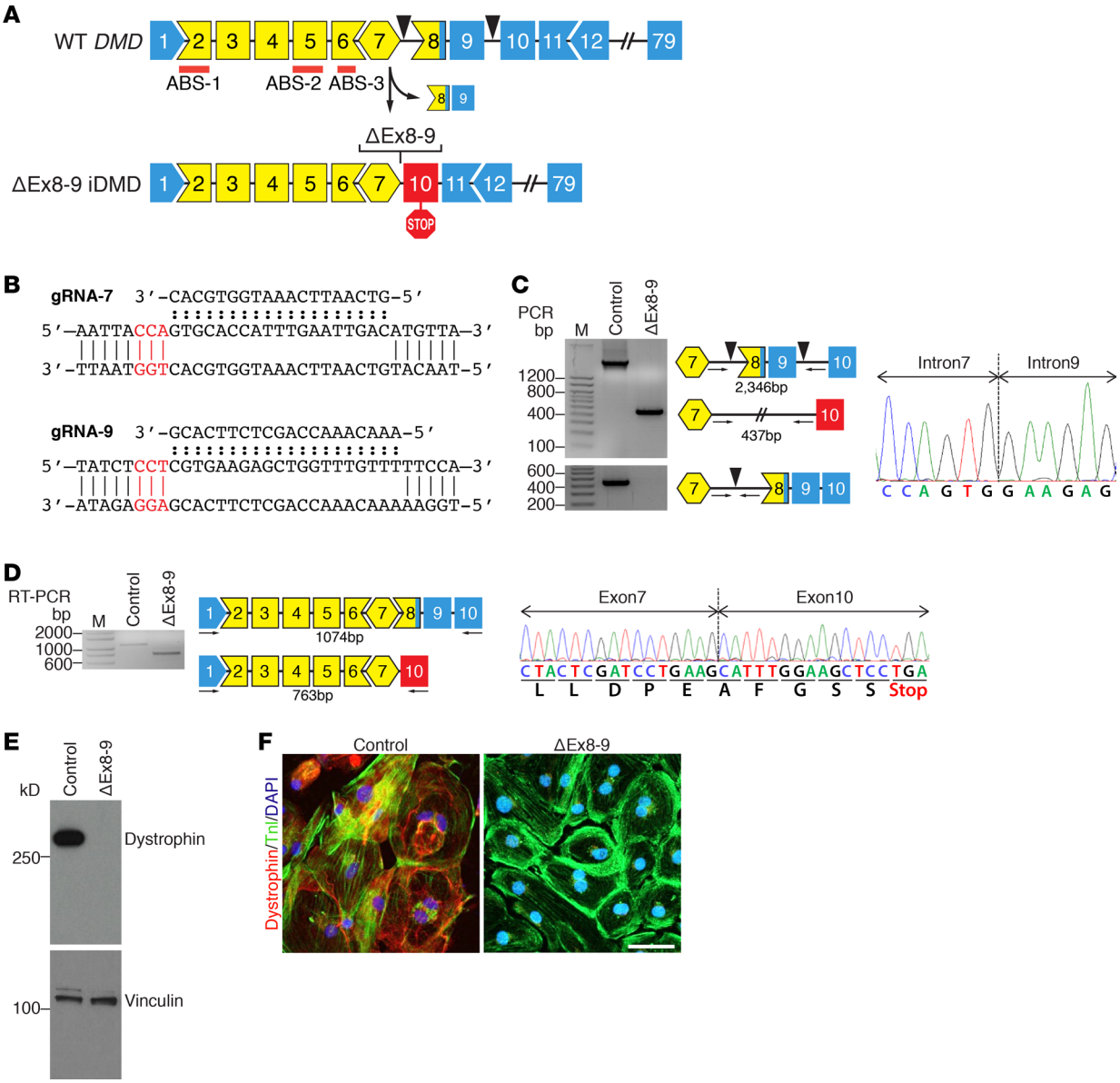

Figure 1. Generating an iDMD model by deleting *DMD* exons 8–9 using CRISPR/Cas9-mediated genome editing. (**A**) Strategy showing CRISPR/Cas9-mediated genomic editing of WT *DMD* to generate ΔEx8-9 iDMD. Shape and color of boxes denoting *DMD* exons indicate reading frame and protein coding domains. Yellow designates actin binding domain-1 (ABD-1). Blue marks part of the central rod domain. Red lines indicate actin binding sites (ABS1, ABS2, and ABS3). Arrowheads mark targeting site of guide RNAs (gRNAs). Stop sign marks exon with stop codon. (**B**) Sequences of gRNAs and their targeting sites within intron 7 (top) and intron 9 (bottom). gRNAs were designed to target the 3′ region of intron 7 (gRNA-7) and 5′ region of intron 9 (gRNA-9). PAM sites are highlighted in red. (**C**) PCR genotyping of control and ΔEx8-9 iDMD induced pluripotent stem cell (iPSC) lines using primers upstream and downstream of the gRNA targeting sites (top) and within intron 7 flanking the gRNA-7 targeting site (bottom). Sequencing of PCR product of ΔEx8-9 iDMD validates splicing of intron 7 to intron 9. PCR primers are indicated by arrows. Arrowhead indicates gRNA targeting site. M denotes marker lane. (**D**) RT-PCR analysis of dystrophin mRNA expression in control and ΔEx8-9 iDMD iPSC–derived cardiomyocytes. Forward primer targeting exon 1 and reverse primer targeting exon 10 were used. Sequencing confirmed splicing of exon 7 to exon 10, introducing a stop-codon. (**E**) Western blot analysis showing dystrophin protein expression in iPSC-derived cardiomyocytes using anti-dystrophin antibody. Vinculin was used as loading control. $n = 7$ for each group. (**F**) Immunocytochemistry representations of iPSC-derived cardiomyocytes with anti-dystrophin (red) and anti–troponin I (green). Nuclei are stained with Hoechst 33342 (blue). Scale bar: 50 μm. $n = 4$ for each group.

as measured by Western blot analysis (Figure 4F and Supplemental Figure 1C). This suggests that deletion of *DMD* exons 7–11, which produces dystrophin lacking amino acids 177–444, results in a truncated form of dystrophin that is degraded.

Functional restoration of iPSC-derived cardiomyocytes by correction of ABD-1 mutations. To assess the consequences of ABD-1 mutations and the effect of correction by genome editing on dystrophin function in muscle,

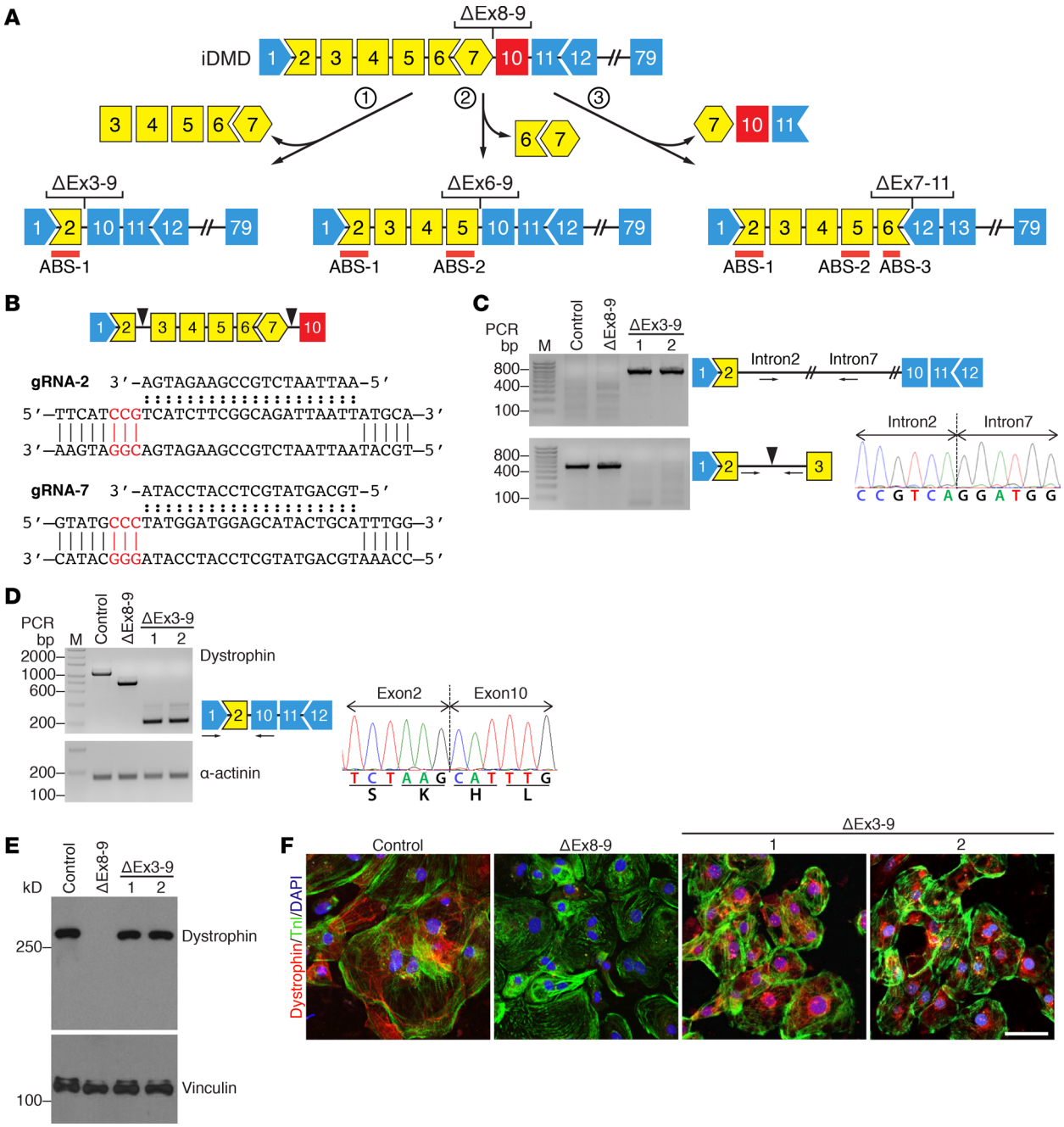

Figure 2. Correcting ΔEx8-9 iDMD by exon deletion to restore dystrophin expression. (**A**) Three strategies were used to correct ΔEx8-9 iDMD by CRISPR/Cas9-mediated genomic editing: (i) deleting exons 3–7 to generate ΔEx3-9, (ii) deleting exons 6–7 to generate ΔEx6-9, and (iii) deleting exons 7–11 to generate ΔEx7-11. Shape and color of boxes denoting *DMD* exons indicate reading frame and protein coding domains. Yellow designates actin binding domain-1 (ABD-1). Blue marks part of the central rod domain. Red lines indicate actin binding sites (ABS1, ABS2, and ABS3). Red exon indicates exon with stop codon. (**B**) Illustration showing deletion of exons 3–7 to generate ΔEx3-9. Sequences of gRNAs and their targeting sites within intron 2 (top) and intron 7 (bottom). gRNAs were designed to target 3′ region of intron 2 (gRNA-2) and 5′ region of intron 7 (gRNA-7). Arrowheads mark targeting site of gRNAs. PAM sites are highlighted in red. (**C**) PCR genotyping of control, ΔEx8-9 iDMD, and two clones of ΔEx3-9 induced pluripotent cell (iPSC) lines using primers upstream and downstream of the gRNA targeting sites (top) and within intron 2 flanking the gRNA-2 targeting site (bottom). Sequencing of PCR product of ΔEx3-9 validates splicing of intron 2 to intron 7. PCR primers are indicated by arrows. Arrowhead indicates gRNA targeting site. M denotes marker lane. (**D**) RT-PCR analysis of dystrophin mRNA expression in control, ΔEx8-9 iDMD, and two clones of ΔEx3-9 iPSC–derived cardiomyocytes. Forward primer targeting exon 1 and reverse primer targeting exon 10 were used. Sequencing confirmed splicing of exon 2 to exon 10 restoring the open reading frame. α-Actinin was used as loading control. (**E**) Western blot analysis showing dystrophin protein expression in iPSC-derived cardiomyocytes using anti-dystrophin antibody. Vinculin was used as loading control. $n = 7$ for control and ΔEx8-9 iDMD, $n = 3$ for ΔEx3-9 clone 1 and ΔEx3-9 clone 2 $n = 7$ for control and ΔEx8-9 iDMD, $n = 3$ for ΔEx3-9 clone 1 and ΔEx3-9 clone 2. (**F**) Immunocytochemistry representations of iPSC-derived cardiomyocytes with anti-dystrophin (red) and anti–troponin I (green). Nuclei are stained with Hoechst 33342 (blue). Scale bar: 50 μm. $n = 4$ for control and ΔEx8-9 iDMD, $n = 2$ for ΔEx3-9 clone 1, and $n = 1$ for ΔEx3-9 clone 2.

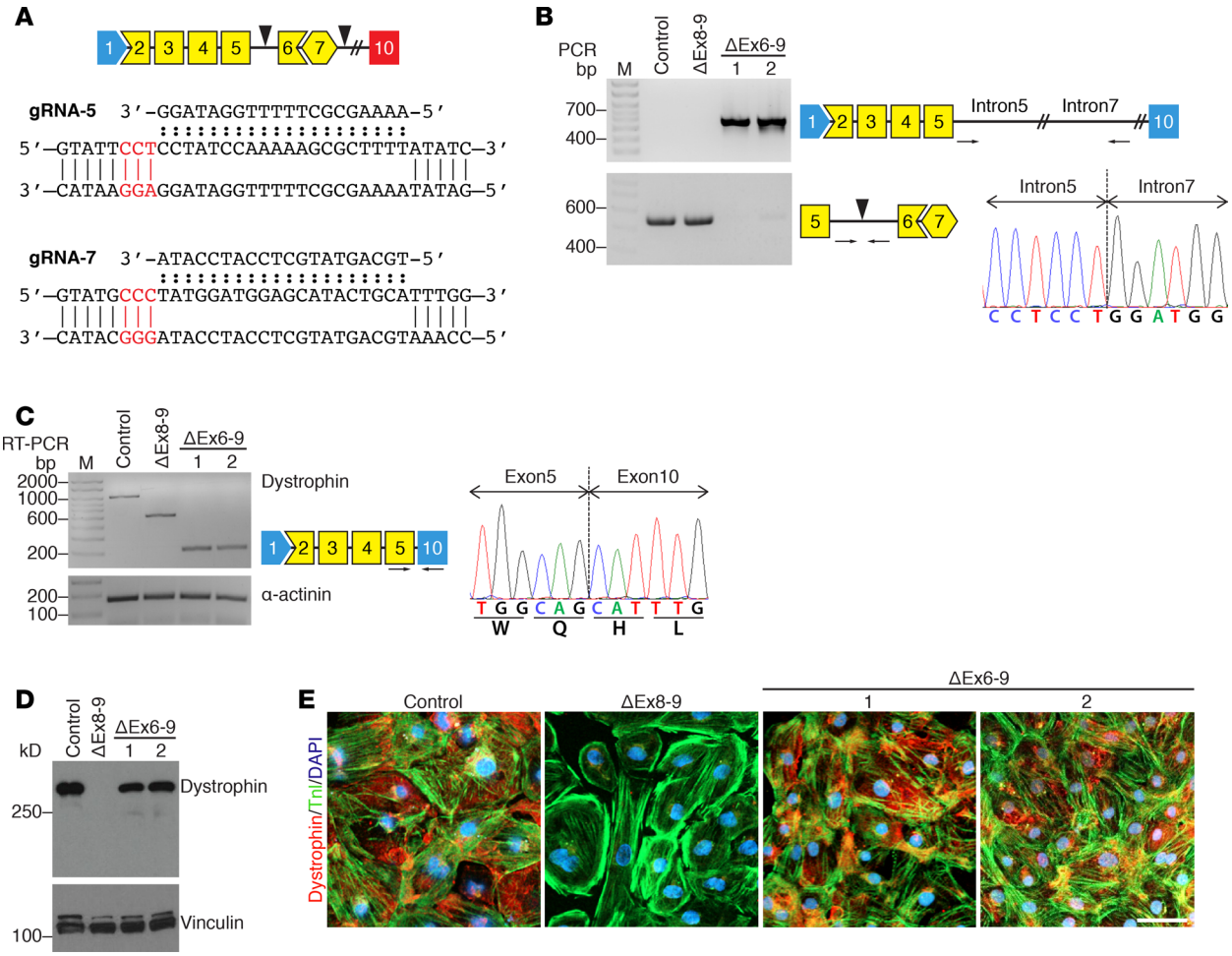

Figure 3. Correcting ΔEx8-9 iDMD by deleting exons 6 and 7 to restore dystrophin protein expression. (**A**) Illustration showing deletion of exons 6–7 to generate ΔEx6-9. Sequences of guide RNAs (gRNAs) and their targeting sites within intron 5 (top) and intron 7 (bottom). gRNAs were designed to target the 3′ region of intron 5 (gRNA-5) and 5′ region of intron 7 (gRNA-7). Arrowheads mark targeting sites of gRNAs. Red exon indicates exon with stop codon. PAM sites are highlighted in red. (**B**) PCR genotyping of control, ΔEx8-9 iDMD, and two clones of ΔEx6-9 induced pluripotent stem cell (iPSC) lines using primers upstream and downstream of the gRNA targeting sites (top) and within intron 5 flanking the gRNA-5 targeting site (bottom). Sequencing of the PCR product of ΔEx6-9 validates splicing of intron 5 to intron 7. PCR primers are indicated by arrows. Arrowhead indicates gRNA targeting site. M denotes marker lane. (**C**) RT-PCR analysis of dystrophin mRNA expression in control, ΔEx8-9 iDMD, and two clones of ΔEx6-9 iPSC–derived cardiomyocytes. Forward primer targeting exon 5 and reverse primer targeting exon 10 were used. Sequencing confirmed splicing of exon 5 to exon 10, restoring the open reading frame. α-Actinin was used as loading control. (**D**) Western blot analysis showing dystrophin protein expression in iPSC-derived cardiomyocytes using anti-dystrophin antibody. Vinculin was used as loading control. $n = 7$ for control and ΔEx8-9 iDMD, $n = 3$ for ΔEx6-9 clone 1 and ΔEx6-9 clone 2. (**E**) Immunocytochemistry representations of iPSC-derived cardiomyocytes with anti-dystrophin (red) and anti–troponin I (green). Nuclei are stained with Hoechst 33342 (blue). Scale bar = 50 μm. $n = 4$ for control and ΔEx8-9 iDMD, $n = 3$ for ΔEx6-9 clone 1 and ΔEx6-9 clone 2.

we analyzed spontaneous Ca^{2+} activity in iPSC-derived cardiomyocytes (Figure 5A). For each CRISPR/Cas9-edited correction, we analyzed data sets from two corrected clones. As expected, we observed that calcium release and reuptake parameters, including time to peak, Ca^{2+} decay rate, and transient duration, were significantly higher in the ΔEx8-9 iDMD iPSC–derived cardiomyocytes compared with isogenic control cells (Figure 5, B–D). Additionally, greater than 50% of the ΔEx8-9 iDMD iPSC–derived cardiomyocytes demonstrated abnormal Ca^{2+} activity, which represents an arrhythmogenic-like phenotype (Figure 5E). In contrast, only 10.7% of the control iPSC–derived cardiomyocytes were desynchronized (Figure 5E).

Corrected ΔEx3-9 iPSC–derived cardiomyocytes displayed normalized Ca^{2+} transient kinetics and decreased asynchronous activity similar to isogenic control cells, suggesting restoration of dystrophin function (Figure 5). Cardiomyocytes derived from ΔEx6-9 iPSCs showed improved Ca^{2+} handling, although not to the level seen with ΔEx3-9 cells (Figure 5). The Ca^{2+} decay rate and Ca^{2+} transient duration were shorter in ΔEx6-9 iPSC–derived cardiomyocytes (Figure 5, C and D), and the number of arrhythmic cells was decreased to 29% compared with ΔEx8-9 iDMD cells (Figure 5E). However, the parameters observed in

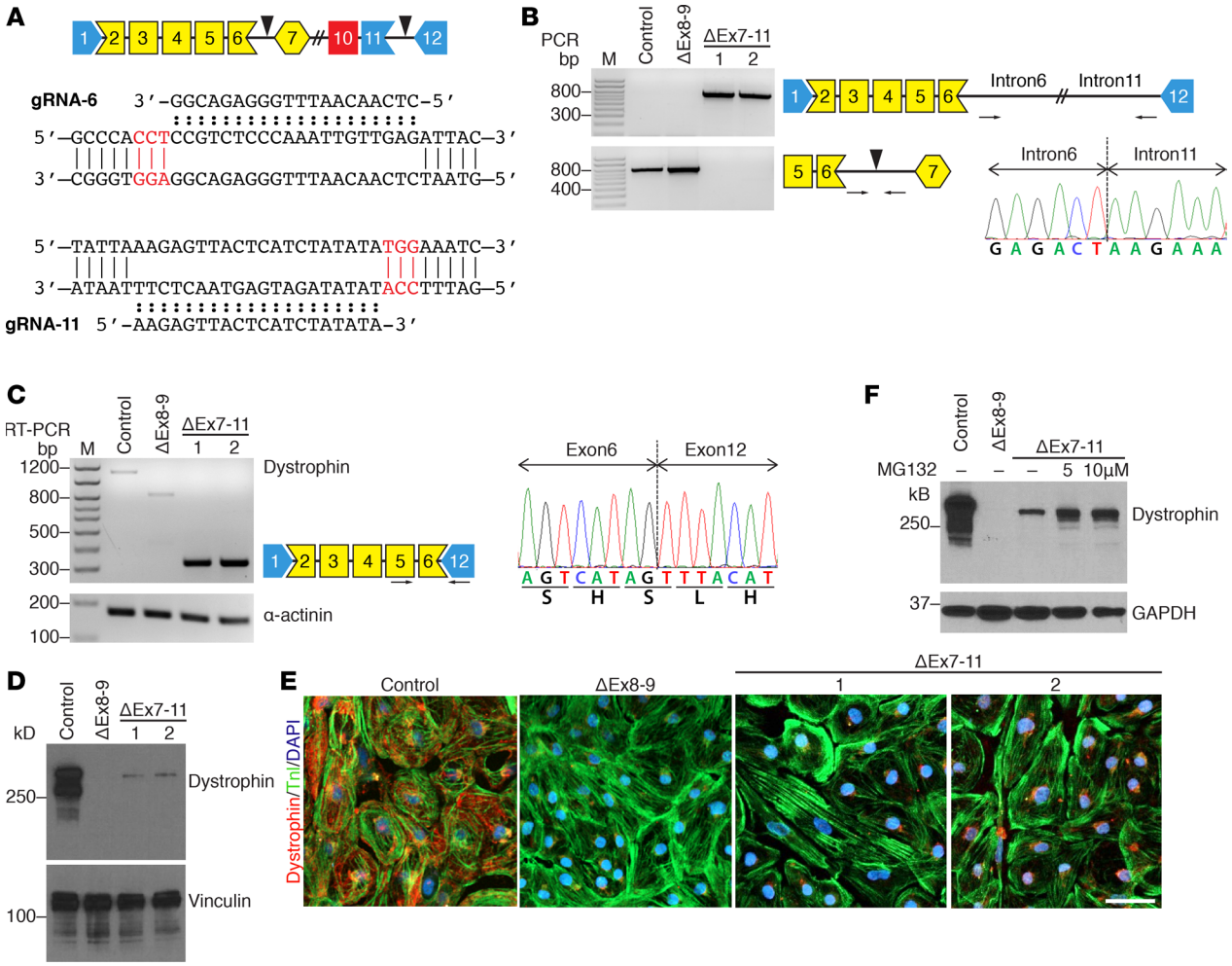

Figure 4. Correcting ΔEx8-9 iDMD by deleting exons 7–11 partially restores dystrophin protein expression. (**A**) Illustration showing deletion of exons 7–11 to generate ΔEx7-11. Sequences of guide RNAs (gRNAs) and their targeting sites within intron 6 (top) and intron 11 (bottom). gRNAs were designed to target the 3′ region of intron 6 (gRNA-6) and 5′ region of intron 11 (gRNA-11). Arrowheads mark gRNA targeting sites. Red exon indicates exon with stop codon. PAM sites are highlighted in red. (**B**) PCR genotyping of control, ΔEx8-9 iDMD, and two clones of ΔEx7-11 induced pluripotent stem cell (iPSC) lines using primers upstream and downstream of the gRNA targeting sites (top) and within intron 6 flanking the gRNA-6 targeting site (bottom). Sequencing of the PCR product of ΔEx7-11 validates splicing of intron 6 to intron 11. PCR primers are indicated by arrows. Arrowhead indicates gRNA targeting site. M denotes marker lane. (**C**) RT-PCR analysis of dystrophin mRNA expression in control, ΔEx8-9 iDMD, and two clones of ΔEx7-11 iPSC–derived cardiomyocytes. Forward primer targeting exon 5 and reverse primer targeting exon 12 were used. Sequencing confirmed splicing of exon 6 to exon 12, restoring the open reading frame. α-Actinin was used as loading control. (**D**) Western blot analysis showing dystrophin protein expression in iPSC-derived cardiomyocytes using anti-dystrophin antibody. Vinculin was used as loading control. $n = 7$ for control and ΔEx8-9 iDMD, $n = 3$ for ΔEx7-11 clone 1 and ΔEx7-11 clone 2. (**E**) Immunocytochemistry representations of iPSC-derived cardiomyocytes with anti-dystrophin (red) and anti–troponin I (green). Nuclei are stained with Hoechst 33342 (blue). Scale bar: 50 μm. $n = 4$ for control and ΔEx8-9 iDMD, $n = 2$ for ΔEx7-11 clone 1, and $n = 1$ for ΔEx7-11 clone 2. (**F**) Western blot analysis of ΔEx7-11 iPSC–derived cardiomyocytes treated with proteasome inhibitor MG132 for 60 hours using anti-dystrophin antibody. GAPDH was used as loading control. $n = 2$.

the ΔEx6-9 iPSC–derived cardiomyocytes did not reach the levels of control iPSC–derived cardiomyocytes. The ΔEx7-11 iPSC–derived cardiomyocytes, similarly to ΔEx6-9 cells, showed improvement in Ca^{2+} release and uptake when compared with ΔEx8-9 iDMD cardiomyocytes (Figure 5, B and C); however, they did not reach control cell levels. iPSC-derived cardiomyocytes with ΔEx7-11 had the highest number of arrhythmic cells, up to 35.9%, among the corrected cell lines (Figure 5E). Taken together, these findings indicate that deletion of exons 3–9 to correct DMD mutations within the 5′-proximal hot spot of the *DMD* gene produces a truncated dystrophin protein with restoration of function.

Further assessment of the functional properties of the iPSC-derived cardiomyocyte cell lines was performed by generating EHM, which displays phenotypic properties of the postnatal myocardium (40). EHM was generated as shown in Supplemental Figure 2A using approximately 95% pure iPSC–derived cardiomyocytes, as measured by α-actinin expression (Supplemental Figure 2B). Consistent with the

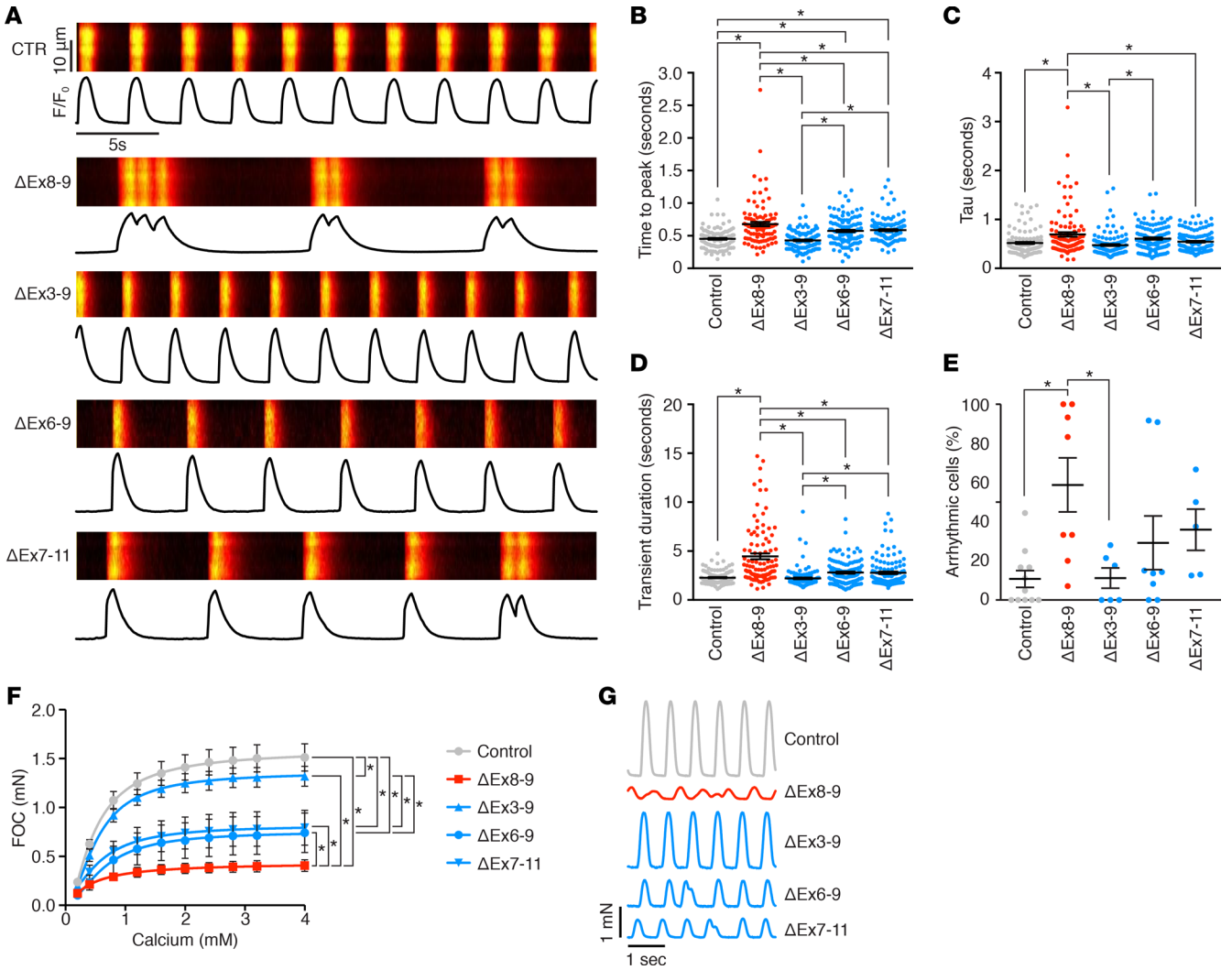

Figure 5. Functional analysis of iPSC-derived cardiomyocytes. (**A**) Representative recordings of spontaneous Ca^{2+} activity of induced pluripotent cell–derived (iPSC-derived) cardiomyocytes loaded with Ca^{2+} indicator Fluo-4AM. Traces show change in fluorescence intensity (F) in relationship to resting fluorescence intensity (F_0). (**B**) Relative time to peak (TTP), (**C**) decay (τ), and (**D**) transient duration (TD), as measured by calcium imaging. (**E**) Arrhythmic iPSC–derived cardiomyocytes were identified based on calcium activity. For all corrected iPSC-derived cardiomyocyte lines (**B**–**E**), data were obtained from 2 independent clones. n = 113 for control; n = 105 for ΔEx8-9 iDMD; n = 129 for ΔEx3-9; n = 121 for ΔEx6-9; and n = 122 for ΔEx7-11 iPSC–derived cardiomyocyte lines from 5–11 independent experiments. Data are represented as mean ± SEM. *P < 0.05 by one-way ANOVA. (**F**) Force of contraction (FOC) recorded in EHM under isometric conditions in the presence of increasing extracellular Ca^{2+}. EHM generated from 2 independent control lines (n = 8), ΔEx8-9 iDMD (n = 6), ΔEx3-9 (n = 14), ΔEx6-9 (n = 3), and ΔEx7-11 (n = 3). *P < 0.05 by two-way ANOVA and Tukey's post-hoc test. (**G**) Representative recordings of EHM contractions from the indicated groups (same EHM as in **F**). Data are represented as mean ± SEM.

calcium handling data, we observed enhanced contractile performance in all corrected cell lines, with the most pronounced effects in ΔEx3-9 EHM (Figure 5F and Supplemental Videos 1–5). Moreover, we observed an increased tendency for arrhythmic contractions in ΔEx8-9 iDMD EHM and a reduction in ΔEx3-9 EHM (Supplemental Figure 2C).

Correction of DMD patient–derived iPSCs by deleting exons 3–9. An iPSC line, referred to as pΔEx3-7, was generated from a DMD patient (SC604A-MD) with a deletion of exons 3–7 in the *DMD* gene. pΔEx3-7 iPSCs are used as patient-in-a-dish models of DMD with a mutation in the ABD-1. To evaluate the effectiveness of exon 3–9 deletion in restoration of cardiomyocyte function, we corrected pΔEx3-7 by deleting exons 8 and 9 to generate pΔEx3-9. Two gRNAs targeting introns 7 and 9 were used to excise exons 8–9, generating pΔEx3-9 iPSCs (Figure 6A). Sequencing of genomic DNA PCR products confirmed the hybrid junction of intron 7 to intron 9 in a single cell–derived iPSC colony (Figure 6B). Both pΔEx3-7 and pΔEx3-9 iPSC lines were differentiated into cardiomyocytes, and RT-PCR was performed with primers targeting the 5′-UTR and exon 10. In pΔEx3-7 iPSC–derived cardiomyocytes, the junction of exon 2 to exon 8 was seen

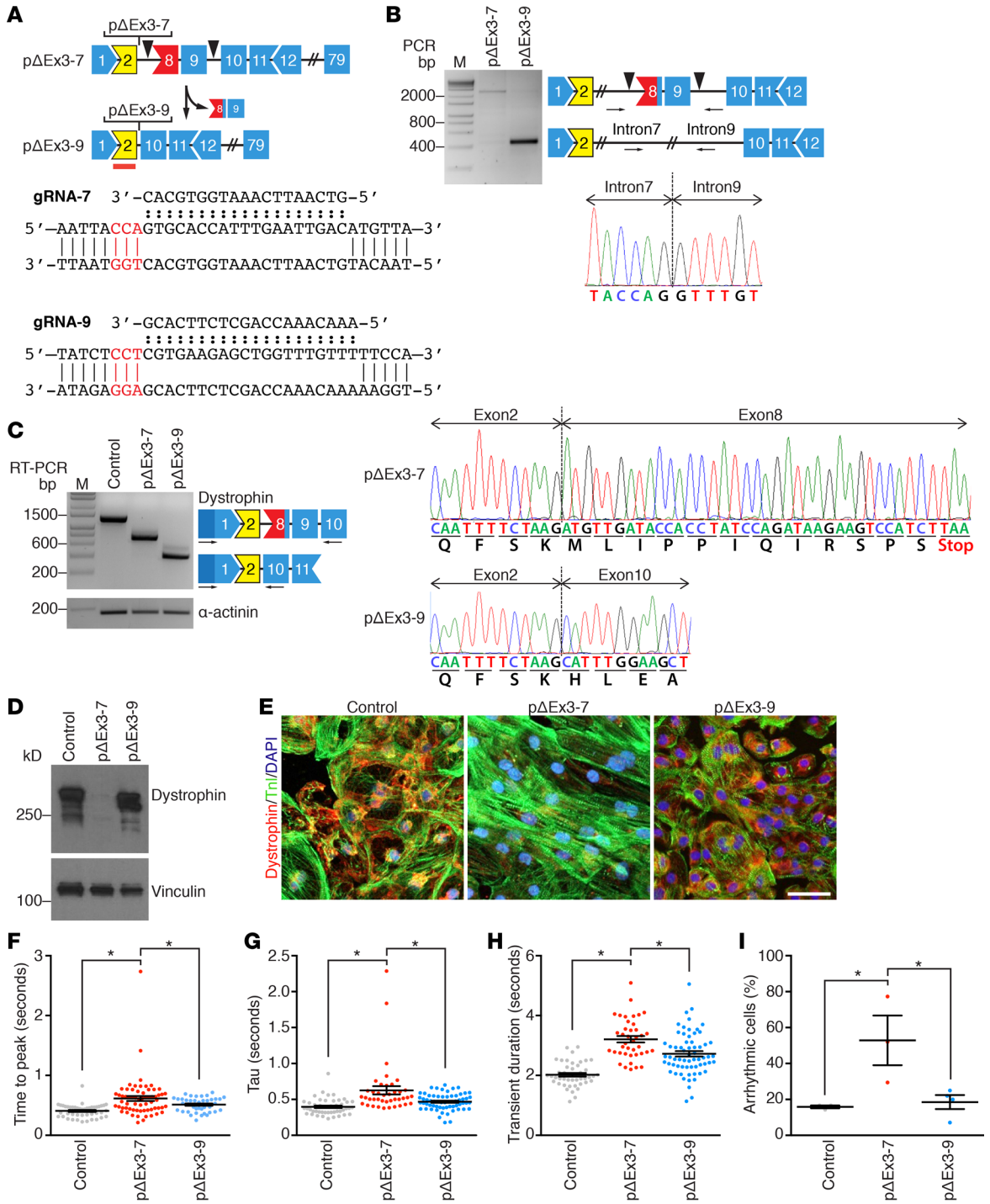

Figure 6. Correction of DMD patient–derived iPSCs by deleting exons 8 and 9. (**A**) Strategy showing CRISPR/Cas9-mediated genomic editing of DMD (Duchene muscular dystrophy) patient (pΔEx3-7) to generate corrected pΔEx3-9 induced pluripotent cell (iPSC) line. Shape and color of boxes denoting *DMD* exons indicate reading frame and protein coding domains. Yellow designates ABD-1. Blue marks part of central rod domain. Red lines indicate ABS1. Arrowheads mark targeting sites of guide RNAs (gRNAs). Red box marks exon with stop codon. Sequences of gRNAs and their targeting sites within intron 7 (top) and intron 9 (bottom). gRNAs were designed to target the 3′ region of intron 7 (gRNA-7) and 5′ region of intron 9 (gRNA-9). PAM sites are highlighted in red. (**B**) PCR genotyping of pΔEx3-7and pΔEx3-9 iPSC lines using primers upstream and downstream of the gRNA targeting sites. Sequencing of PCR product of pΔEx3-9 validates splicing of intron 7 to intron 9. PCR primers are indicated by arrows. Arrowheads mark targeting sites of gRNAs. M denotes marker lane. (**C**) RT-PCR analysis of dystrophin mRNA expression in control, pΔEx3-7, and pΔEx3-9 iPSC–derived cardiomyocytes. Forward primer targeting 5′UTR and reverse primer targeting exon 10 were used. Sequencing of pΔEx3-7 confirmed splicing of exon 2 to exon 8, introducing a stop-codon. Sequencing pΔEx3-9 confirmed splicing of exon 2 to exon 10, restoring the open reading frame. α-Actinin was used as loading control. (**D**) Western blot analysis showing dystrophin protein expression in iPSC-derived cardiomyocytes using anti-dystrophin antibody. Vinculin was used as loading control. n = 7 for control, n = 3 for pΔEx3-7, and n = 3 for pΔEx3-9. (**E**) Immunocytochemistry representations of iPSC-derived cardiomyocytes with anti-dystrophin (red) and anti–troponin I (green). Nuclei are stained with Hoechst 33342 (blue).

Scale bar: 50 μm. *n* = 4 for control, *n* = 2 for pΔEx3-7, and *n* = 2 for pΔEx3-9. (**F**) Relative time to peak (TTP), (**G**) decay (τ), (**H**) transient duration (TD), and (**I**) percent of arrhythmic cells were measured based on calcium activity of control (*n* = 45), DMD patient pΔEx3-7 (*n* = 40), and corrected pΔEx3-9 (*n* = 65) iPSC–derived cardiomyocytes from 3–5 independent experiments. Data are represented as mean ± SEM. $^*P < 0.05$ by one-way ANOVA (**F**–**H**).

by sequencing of the RT-PCR product (Figure 6C). In corrected pΔEx3-9 iPSC–derived cardiomyocytes, the junction of exon 2 to exon 10 was demonstrated by sequencing the RT-PCR product (Figure 6C). Western blot analysis showed a low level of dystrophin expression in DMD pΔEx3-7 iPSC–derived cardiomyocytes (Figure 6D). This is consistent with previous reports showing low levels of dystrophin protein expression in patients lacking exons 3–7 due to reinitiation of translation at an in-frame start codon in exon 8 (42, 43). Corrected pΔEx3-9 iPSC–derived cardiomyocytes showed dystrophin expression similar to normal control cardiomyocytes (Figure 6D). These findings were confirmed by immunocytochemistry (Figure 6E).

Spontaneous Ca^{2+} activity was assessed in these patient-derived cells as a measure of iPSC-derived cardiomyocyte functionality (Figure 6, F–I). In pΔEx3-7 DMD iPSC–derived cardiomyocytes, Ca^{2+} time to peak and time to half decay were elevated (Figure 6, F and G). This caused an overall slower Ca^{2+} transient (Figure 6H) and elevated the number of arrhythmic cells, up to 53% (Figure 6I). Corrected pΔEx3-9 iPSC–derived cardiomyocytes had significantly improved time to peak and faster Ca^{2+} decay (Figure 6, F and G). Although these parameters of the corrected pΔEx3-9 iPSC–derived cardiomyocytes did not reach normal control levels, the number of arrhythmic cells was 18.5%, similar to control iPSC–derived cardiomyocytes (Figure 6I). These findings show improved iPSC-derived cardiomyocyte function after genomic editing to excise exons 3–9 of the *DMD* gene in DMD patient–derived iPSCs.

Discussion

Dystrophin protein serves as a muscular shock absorber by providing a structural link between the cytoskeleton and the extracellular matrix to maintain muscle integrity. Essential regions of the dystrophin protein are located at both ends of the protein; the amino-terminus contains ABD-1, and the carboxy-terminus includes binding sites for components of the dystrophin associated protein complex, such as sarcoglycans and dystroglycans. Genomic mutations in the *DMD* gene encoding nonessential regions have been excised by exon skipping and deletion to restore functional, albeit truncated, dystrophin protein. Here, we use CRISPR/Cas9-mediated editing to selectively delete exons 3–9 of the *DMD* gene encoding part of the essential ABD-1 region. With precision genomic editing, we can modify the essential amino-terminal region and restore dystrophin expression and cardiomyocyte function.

To provide an isogenic control iPSC line for our studies, we generated an iDMD model (ΔEx8-9) by deleting *DMD* exons 8 and 9 in a healthy donor–derived iPSC line. We confirmed ΔEx8-9 iDMD iPSCs as a model of DMD by showing that cardiomyocytes derived from these cells do not express dystrophin protein and display arrhythmias attributable to impaired Ca^{2+} cycling. The lack of dystrophin results in the loss of linkage between the extracellular matrix and the actin cytoskeleton, destabilizing membrane proteins and resulting in generation of ROS and excessive Ca^{2+} entry (4). Consistent with our findings, it was shown that cardiomyocytes differentiated from DMD iPSCs have slower Ca^{2+} cycling (44). Additionally, others have reported cellular abnormalities such as elevated levels of resting Ca^{2+}, mitochondrial damage, and apoptosis in DMD-derived iPSC cardiomyocytes (45). Complementary to the phenotype of DMD iPSC–derived cardiomyocytes, DMD patients develop cardiomyopathy, fibrosis, and cardiac arrhythmias (46). Taken together, this corroborates our findings that deletion of exons 8 and 9 of the *DMD* gene in normal iPSCs generates an iDMD model and that cardiomyocytes derived from ΔEx8-9 iDMD serve as a model of "DMD in a dish".

Our approach is to use CRISPR/Cas9-mediated genomic editing to restore the open reading of the *DMD* gene and measure the functional outcome of truncated dystrophin in muscle. One of the potential issues of using CRISPR/Cas9 editing is the occurrence of unintended, off-target, genomic cleavage (47). Reassuringly, previous reports showed that CRISPR/Cas9-modified human iPSC clones do not exhibit elevated off-target mutation rates, supporting the use of edited iPSC clones for disease modeling (48, 49). Nevertheless, we recognize that Cas9 nuclease poses a potential safety concern for clinical applicability, and we acknowledge that whole-genome sequencing should be performed in future in vivo studies to identify potential off-target changes in the genome.

Mutations in the ABD-1 region are genotypically and phenotypically variable in patients (50). In some cases, out-of-frame ABD-1 mutations display a BMD phenotype, most likely due to the presence of an

alternative translation initiation site in exons 6 or exon 8. Interestingly, it was shown that deletion of exon 2 activates an alternative translation initiation site in exon 6 to generate truncated dystrophin (30). However, duplication of exon 2, which results in a stop codon within the duplicated exon 2, does not activate an alternative translation initiation site. To correct the duplication of exon 2, a U7 small nuclear RNA was used against exon 2 to skip one or both copies of exon 2, generating either full-length or truncated dystrophin (30). Another approach used to correct exon 2 duplication was to use CRISPR/Cas9-mediated editing with one gRNA directed against a duplicated intronic region, resulting in precise deletion of one of the duplicated exons and restoration the *DMD* gene (31). Patients with deletion of exons 3–7 display variable phenotypes, depending on whether the alternative translation initiation site in exon 8 is used (43, 50). However, in general, patients with ABD-1 mutations display a severe BMD phenotype or are diagnosed as DMD. Studies using micro- and minidystrophins as therapeutic approaches to treat DMD showed that the truncated dystrophins remain functional if they lack portions of the central rod domain (51). However, restoration of muscle function by expression of microdystrophin in the *mdx* mouse model of DMD must include an intact ABD-1 region (52).

Correcting the ABD-1 mutation in DMD is not exclusively based on restoring the open reading frame. Functional assessment of the truncated dystrophin isoforms that are modified in the ABD-1 region is essential. There are three ABSs localized within the ABD-1 region: ABS1 (amino acids 18–27 encoded by exon 2); ABS2 (amino acids 88–116 encoded by exon 5); and ABS3 (amino acids 131–147 encoded by exon 6). Our three approaches to correct ΔEx8-9 iDMD iPSCs by CRISPR/Cas9-mediated editing produced different modifications to the dystrophin ABD-1 region, such that corrected ΔEx3-9 retained the ABS1; corrected ΔEx6-9 retained both ABS1 and ABS2; and corrected ΔEx7-11 retained all three ABSs. Unexpectedly, the ΔEx7-11 correction, which retained most of the ABD-1 region, created the least-stable protein, showing minimal restoration of function. The ΔEx7-11 iPSC–derived cardiomyocytes expressed low levels of dystrophin protein compared with isogenic control cells and the corrected ΔEx3-9 and ΔEx6-9 lines. The decrease in dystrophin expression in the ΔEx7-11 iPSC–derived cardiomyocytes resulted in slower Ca^{2+} cycling and higher propensity for arrhythmias. In eDystrophin (http://edystrophin.genouest.org), a database dedicated to human dystrophin variants produced by in-frame DMD gene mutations, a patient with the ΔEx7-11 *DMD* deletion was annotated as DMD. It has also been reported that a single missense point mutation in exon 11 causes DMD protein misfolding and dysfunction, resulting in a BMD phenotype (53). Therefore, we conclude that, although the deletion of exons 7–11 maintains the open reading frame of the *DMD* gene, the absence of amino acids 178–444 causes protein misfolding and subsequent degradation. Indeed, by inhibiting proteasome activity, truncated dystrophin protein increased in ΔEx7-11 iPSC–derived cardiomyocytes. Furthermore, it was reported that, when recreated in vitro, point mutations in the ABD-1 region that cause a human DMD phenotype are associated with decreased dystrophin protein levels due to proteasomal degradation (41).

Correction of DMD ΔEx8-9 mutation by deleting exons 6–9 retained ABS1 and ABS2 and improved Ca^{2+} activity in cardiomyocytes, but it did not fully restore function to control levels. Shorter time to peak in these cells indicates faster Ca^{2+} release from the intracellular stores. However, slower Ca^{2+} decay in these cells compared with control cells suggests that their Ca^{2+} reuptake system was not completely restored, resulting in arrhythmias. A similar strategy was applied to correct the ABD-1 mutation in a golden retriever dog model of DMD, which harbors a mutation in the exon 7 splice site. Some functional improvement was seen when exons 6–8 were deleted, resulting in splicing of exon 5 to 9 or to exon 10 due to occurrence of a cryptic splice site in exon 9 (32, 33).

Among the three genome-editing correction strategies we tested, ΔEx3-9 — which generated the truncated dystrophin lacking amino acid residues 32–320 — was the most effective in restoring functionality of iPSC-derived cardiomyocytes. We used CRISPR/Cas9 to create ΔEx3-9 using ΔEx8-9 iDMD or DMD patient–derived pΔEx3-7 iPSCs, and we restored iPSC-derived cardiomyocyte function in both ΔEx3-9 corrected cell lines. ΔEx3-9 produces truncated dystrophin that retains ABS1. Consistent with our findings, it was shown that overexpressing the dystrophin isoform lacking ABS2 and ABS3 prevents severe dystrophy in *mdx* mice (54). In addition, by surveying different databases, Nakamura and colleagues identified 15 patients with an exon 3–9 deletion, 11 of whom were asymptomatic or diagnosed as BMD (38). In fact, one of these patients is a competitive badminton player and was asymptomatic until he was diagnosed with BMD at age 67 (37). His dystrophin level was recorded using two different dystrophin antibodies: as 47%

of the control level using a C-terminus antibody and 62% of the control level using a rod domain antibody. Another of these patients expressed only 15% of normal dystrophin levels and showed a slight decrease in cardiac function at age 21, with no obvious skeletal muscle involvement (38). Similarly, in mouse models, at least 20% of full-length or central rod domain–deleted dystrophin expression is required to rescue the *mdx* phenotype (55, 56). In human mutations involving the 5′-proximal region of the *DMD* gene, 30% or more of dystrophin expression is required to prevent diagnosis of muscular dystrophy in X-linked dilated cardiomyopathy patients (57). Taken together, these reports show in both mice and humans that deletion of exons 3–9 of the *DMD* gene produces a stable, albeit truncated dystrophin protein capable of maintaining function even when expressed at low levels (37, 38, 54).

The functional relevance of the ΔEx3-9 mutation and its potential therapeutic superiority compared with ΔEx6-9 and ΔEx7-11 was further underscored by phenotypic screening in EHM. All three models resulted in improved contractile performance compared with the iDMD model; however, ΔEx3-9-EHM showed the most enhanced contractile force and lowest propensity for arrhythmic contractions. This suggests deletion of exons 3–9 of the *DMD* gene as a practical candidate for exon deletion that could be applicable to approximately 7% of DMD patients' mutations (38). The other two correction strategies that deleted exons 6–9 or 7–11 could each potentially correct approximately 2% of DMD patients' mutations based on the UMD-DMD database (8). Although shown as a possible gene therapy approach for correcting DMD, we are aware that deletion of exons 3–9 of the *DMD* gene generates a large genome deletion up to approximately 150 kb. To this point, large genome deletions by CRISPR/Cas9-mediated editing of up to 725 kb of the *DMD* gene have been previously reported to delete exons 45–55 in human cells in vitro and in a humanized DMD mouse model in vivo (16, 22, 58). Ultimately, the efficiency of CRISPR/Cas9-mediated deletion of exons 3–9 of the *DMD* gene by two gRNAs and the function of the truncated dystrophin needs to be tested in an ABD-1 mutant DMD mouse model.

In summary, our human iPSC results provide evidence that deletion of exons 3–9 in the *DMD* gene restores muscle function and is applicable for using CRIPSR/Cas9 genomic editing to correct ABD-1 mutations that were previously not addressed. The functional properties of these dystrophin ABD-1 mutations will dictate the most efficacious CRISPR/Cas9 strategy for possible genomic editing to correct DMD mutations within the proximal hot spot of the *DMD* gene, allowing effective restoration of dystrophin function.

Methods

Human iPSC maintenance, nucleofection, and differentiation. Human healthy donor iPSCs were reprogrammed from peripheral blood mononuclear cells with CytoTune-iPS Sendai Reprograming Kit (catalog A16518; Thermo Fisher Scientific). Human Muscular Dystrophy iPS Cell Line (catalog SC604A-MD; Systems Biosciences Inc.) was referred to as pΔEx3-7. Human iPSCs were cultured in mTeSR1 media (catalog 05850; Stemcell Technologies) and passaged approximately every 3–4 days (1:12-1:18 split ratio). One hour before nucleofection, iPSCs were treated with 10 μM ROCK inhibitor, Y-27632 (catalog S1049, Selleckchem), and dissociated into single cells using Accutase (catalog A6964; Innovative Cell Technologies Inc.). iPSCs (1×10^6) were mixed with 6 μg total of pSpCas9(BB)-2A-GFP (PX458) from Feng Zhang (MIT, Cambridge, Massachusetts, USA) Addgene plasmid 48138 (59), which contains gRNA as indicated, and then nucleofected using the P3 Primary Cell 4D-Nucleofector X kit (catalog V4XP-3024; Lonza) according to manufacturer's protocol. After nucleofection, iPSCs were cultured in mTeSR1 media supplemented with 10 μM ROCK inhibitor and 100 μg/ml Primocin (InvivoGen), and the next day, the media was switched to fresh mTeSR1. Three days after nucleofection, GFP(+) and GFP(–) cells were sorted by FACS and subjected to genotyping by PCR. Single clones derived from GFP(+) iPSCs were picked, genotyped, and sequenced. iPSCs were induced to differentiate into cardiomyocytes, using a previously described protocol with modifications. When cells reached ~80% confluency, the medium was changed to CDM3 (60) every other day until day 10. On days 0–2, medium was supplemented with 4 μM of CHIR99021 (catalog S2924; Selleckchem); on days 2–4, medium was supplemented with 2 μM WNT-C59 (catalog S7037; Selleckchem). On day 10 after differentiation initiation, media was changed to RPMI 1640 medium, no glucose (catalog 11879020; Thermo Fisher Scientific), supplemented with B27-supplement (catalog 17504044; Thermo Fisher Scientific) for 10 days. On day 20, media was switched to RPMI 1640 medium (catalog 11875093; Thermo Fisher Scientific), supplemented with B27-supplement. Cardiomyocytes were used for experiments on days 30–40 after initiation of differentiation.

Genomic DNA isolation. Genomic DNA of human iPSCs was isolated using DirectPCR (Cell) (catalog 302-C; Viagen) according to manufacturer's recommendations.

RT-PCR. RNA from iPSC-derived cardiomyocytes was isolated using TRIzol (catalog 15596026; Thermo Fisher Scientific) and extracted with Direct-zol RNA MiniPrep kit (catalog R2050; Zymo Research) according to manufacturer's protocol. cDNA was synthesized using iScript gDNA Clear cDNA Synthesis Kit (catalog 1725034; Bio-Rad) according to manufacturer's instructions. cDNA (2 μg per reaction) was used for RT-PCR reaction using Taq polymerase for 40 cycles. Primer pairs used for human *DMD* RT-PCR were as follows:

Exon 1 forward, 5′-CTTTGGTGGGAAGAAGTAGAGGACTG-3′; 5′-UTR forward, 5′-CTTTCCCCCTACAGGACTCAG-3′; exon 5 forward, 5′-TTGGAAGTACTGACATCGTAGATGGA-3′; exon 10 reverse, 5′-CTCAGCAGAAAGAAGCCACGATAATA-3′; exon 12 reverse, 5′-TGTTAGCCAGTCATTCAACTCTTTCA-3′.

PCR products for exon 1 forward and exon 10 reverse primers were 1,073 bps in control (ctrl) iPSC-derived cardiomyocytes (iPSC-CM), 762 bps in ΔEx8-9 iDMD iPSC-CM, and 206 bps in ΔEx3-9 iPSC-CM. PCR products for exon 5 forward and exon 10 reverse primers were 797 bps in ctrl iPSC-CM, 486 bps in ΔEx8-9 iDMD iPSC-CM, and 194 bps in ΔEx6-9 iPSC-CM. PCR products for exon 5 forward and exon 12 reverse primers were 1,115 bps in ctrl iPSC-CM, 804 bps in ΔEx8-9 iDMD iPSC-CM, and 314 bps in ΔEx7-11 iPSC-CM. PCR products for 5′-UTR forward and exon 10 reverse primers were 1,345 bps in ctrl iPSC-CM, 748 bps in pΔEx3-7 iPSC-CM, and 544 bps in pΔEx3-9 iPSC-CM. PCR products were run on 1.5% agarose gel, excised, and sequenced. The primer pair used for human α-actinin control is: ACTN2 forward, 5′-CAACTTCAACACGCTGCAGACCAA-3′; ACTN2 reverse, 5′-AAGCGCTCCAGTCTTCGAATCTCA-3′.

Dystrophin Western blot analysis. iPSC-CMs were collected in cold PBS on ice, centrifuged, and lysed with RIPA lysis buffer: 150 mM NaCl (Sigma-Aldrich), 0.5% sodium deoxycholate (Sigma-Aldrich), 0.1% SDS (Thermo Fisher Scientific), 5% glycerol (Sigma-Aldrich), 50 mM Tris-HCl (Research Products International) pH 7.4, 1% Nonidet P40 (Sigma-Aldrich). Samples were needle-homogenized, big clumps were removed by centrifugation, and supernatant was incubated at 95°C for 10 minutes in the presence of Laemmli sample buffer (catalog 161-0747; Bio-Rad). Protein (10 μg per sample) was separated on Mini-PROTEAN TGX 4-20% precast gels (Bio-Rad) for 3 hours at 100 V. Proteins were transferred to PVDF membrane at 100 V for 1.5 hours. Membranes were probed with mouse anti-dystrophin antibody MANDYS8 (1:1,000) (catalog D8168; Sigma-Aldrich) and with mouse anti-vinculin antibody, hVIN-1 (1:1,000) (catalog V9131; Sigma-Aldrich). For analysis of DEx7-11 iPSC–derived cardiomyocytes treated with proteasome inhibitor MG132, membranes were cut; the upper portion was probed with mouse MANDYS8 anti-dystrophin antibody (1:1,000) (catalog #D8168; Sigma-Aldrich) and the lower portion with mouse anti-GAPDH antibody (1:1,000) (catalog MAB374; clone 6C5, EMD Milipore). Goat anti–mouse HRP–conjugated secondary antibodies were used (1:10,000) (catalog 172-1011; Bio-Rad).

Dystrophin and troponin-I immunocytochemistry. iPSC-derived cardiomyocytes (1×10^5) seeded on 12-mm coverslips coated with poly-D-lysine and Matrigel (catalog 354248; Corning) were removed from culture media and fixed in cold acetone (10 minutes, –20°C). Following fixation, coverslips were equilibrated in phosphate-buffered saline, pH 7.3 (PBS), and then blocked for 1 hour with serum cocktail (2% normal horse serum/2% normal donkey serum/0.2% BSA/PBS). Excess blocking cocktail was removed, and dystrophin/troponin primary antibody cocktail, mouse anti-dystrophin (1:800) (catalog D8168; clone MANDYS8, Sigma-Aldrich), and rabbit anti–troponin-I (1:200) (catalog sc-15368; clone H170, Santa Cruz Biotechnology) in 0.2% BSA/PBS was applied without an intervening wash. Following overnight incubation at 4°C, unbound primary antibodies were removed with PBS washes, and coverslips were probed for 1 hour with secondary antibodies, biotinylated horse anti–mouse IgG (1:200) (catalog BA-2000, Vector Laboratories) and fluorescein-conjugated donkey anti-rabbit IgG (1:50) (catalog 711-095-152, Jackson ImmunoResearch) diluted in 0.2% BSA/PBS. Unbound secondary antibodies were removed with PBS washes, and final dystrophin labeling was done with 10-minute incubation of rhodamine avidin DCS (1:60) (Vector Laboratories) diluted in PBS. Unbound rhodamine was removed with PBS washes, nuclei were counterstained with 2 μg/ml Hoechst 33342 (Molecular Probes), and coverslips were inverted onto slides overlaid with Vectashield fluorescent mounting media (Vector Laboratories).

Calcium imaging. iPSC-derived cardiomyocytes were dissociated with TrypLE (catalog 12605036; Thermo Fisher Scientific) and single cells were plated at low density on Matrigel-coated 35 mm glass-bottom dishes (catalog 150680, Thermo Fisher Scientific). Ca^{2+} handling was measured 3–4 days after plating. To monitor changes in cytoplasmic Ca^{2+}, iPSC-derived cardiomyocytes were loaded with 5 μM fluorescent Ca^{2+} indicator Fluo-4 AM (catalog F14201; Thermo Fisher Scientific) in the presence of 2 mmol/l of Pluronic F-127 for 20 minutes in Tyrode's solution (140 mM NaCl, 5.4 mM KCl, 1 mM

$MgCl_2$, 10 mM glucose, 1.8 mM $CaCl_2$, 10 mM HEPES, pH 7.4). The Ca^{2+} transients of spontaneously beating iPSC–derived cardiomyocytes were imaged at 37°C using a Zeiss LSM880 confocal system using a 40× oil immersion objective. Ca^{2+} transients were processed and analyzed using ImageJ (NIH) and pClamp 10.2 software (Axon Instrument). For the calcium release phase, we calculated time to peak (time from baseline to maximal point of the transient). For evaluation of calcium reuptake, the total transient time and time of Ca^{2+} decay were evaluated. The time of Ca^{2+} decay was calculated by fitting a first-order exponential decay to the calcium reuptake phase of the calcium transient profile. Cells were considered arrhythmic if they had one or more asynchronized Ca^{2+} transients. For each experimental group, we analyzed cells from at least three independent sets of iPSC-derived cardiomyocytes.

EHM. EHM was constructed as previously reported (40) from iPSC-derived cardiomyocytes of iDMD (ΔEx8-9; $n = 6$) and the corrected lines (ΔEx3-9, $n = 14$; ΔEx6-9, $n = 3$; ΔEx7-11, $n = 3$). All lines were adapted to a published cardiomyocyte differentiation protocol (40), which resulted in high and homogeneous cardiomyocyte purity in the different iPSC cultures, showing 95% ± 1% α-actinin positive ($ACTN2^+$) cardiomyocytes by flow cytometry ($n = 8$). For EHM construction, 1×10^6 iPSC-derived cardiomyocytes were mixed with 0.5×10^6 human foreskin fibroblasts (catalog SCRC-1041; ATCC). EHM was cultured for 4 weeks, followed by isometric force measurements under electrical field stimulation (1.5 Hz) at 37°C in Tyrode's solution. Two healthy donor–derived iPSC lines were included as a reference: control (WT) shiPS9-1 (provided by Daniel Garry, University of Minnesota, Minneapolis, Minnesota, USA) ($n = 4$) and hiPSC-G1 line ($n = 4$) (40).

Statistics. Statistical analysis was assessed by one-way ANOVA or two-way ANOVA and Tukey's post-hoc test where indicated. Data are shown as mean ± SEM. $P < 0.05$ value was considered statistically significant.

Study approval. All methods were performed in accordance with University of Texas Southwestern and University Medical Center Göttingen regulatory guidelines. Human peripheral blood draw was collected from individuals under signed informed consent prior to the participation in the study.

Author contributions

VK, CL, RBD, and ENO designed the concept. VK, SK, MT, JMS, CL, JWS, WHZ, RBD, and ENO designed experiments. VK, SK, MT, and JMS performed the experiments. VK, RBD, WHZ, and ENO wrote and edited the manuscript.

Acknowledgments

We thank Daniel J. Garry for providing the patient-derived iPSC line, Cristina E. Rodriguez for technical help, and Jose Cabrera for assistance with graphics. This work was supported by grants from the NIH (HL-130253, HL-077439, DK-099653, and AR-067294), Senator Paul D. Wellstone Muscular Dystrophy Cooperative Research Center (grant U54 HD 087351), Parent Project Muscular Dystrophy Award, and the Robert A. Welch Foundation (grant 1-0025 to ENO). VK was awarded a postdoctoral fellowship from the Senator Paul D. Wellstone Muscular Dystrophy Cooperative Research Center. MT and WHZ are supported by the DZHK (German Center for Cardiovascular Research), the German Federal Ministry for Science and Education (BMBF FKZ 01GN0819 and 13GW0007A [CIRM-ET3]), the German Research Foundation (DFG ZI 708/10-1; SFB 937 TP18; SFB 1002 TPs C04 and S1; IRTG 1618 RP12), and the Foundation Leducq. We thank Daria Reher from the SFB1002 Service Unit (S1) for cardiomyocyte production for the tissue engineering work.

Address correspondence to: Eric N. Olson, University of Texas Southwestern Medical Center, 5323 Harry Hines Boulevard, Dallas, Texas 75390, USA. Phone: 214.648.1187; Email: Eric.Olson@UTSouthwestern.edu.

C. Long's present address is: Leon H. Charney Division of Cardiology, New York University School of Medicine, New York, New York, USA.

1. Campbell KP, Kahl SD. Association of dystrophin and an integral membrane glycoprotein. *Nature*. 1989;338(6212):259–262.
2. Le Rumeur E. Dystrophin and the two related genetic diseases, Duchenne and Becker muscular dystrophies. *Bosn J Basic Med Sci*. 2015;15(3):14–20.
3. Monaco AP, Bertelson CJ, Liechti-Gallati S, Moser H, Kunkel LM. An explanation for the phenotypic differences between patients bearing partial deletions of the DMD locus. *Genomics*. 1988;2(1):90–95.
4. Allen DG, Whitehead NP, Froehner SC. Absence of dystrophin disrupts skeletal muscle signaling: roles of Ca^{2+}, reactive oxy-

gen species, and nitric oxide in the development of muscular dystrophy. *Physiol Rev*. 2016;96(1):253–305.
5. Kyrychenko S, et al. Hierarchical accumulation of RyR post-translational modifications drives disease progression in dystrophic cardiomyopathy. *Cardiovasc Res*. 2013;97(4):666–675.
6. Beggs AH, et al. Exploring the molecular basis for variability among patients with Becker muscular dystrophy: dystrophin gene and protein studies. *Am J Hum Genet*. 1991;49(1):54–67.
7. Aartsma-Rus A, Van Deutekom JC, Fokkema IF, Van Ommen GJ, Den Dunnen JT. Entries in the Leiden Duchenne muscular dystrophy mutation database: an overview of mutation types and paradoxical cases that confirm the reading-frame rule. *Muscle Nerve*. 2006;34(2):135–144.
8. Tuffery-Giraud S, et al. Genotype-phenotype analysis in 2,405 patients with a dystrophinopathy using the UMD-DMD database: a model of nationwide knowledgebase. *Hum Mutat*. 2009;30(6):934–945.
9. Bladen CL, et al. The TREAT-NMD DMD Global Database: analysis of more than 7,000 Duchenne muscular dystrophy mutations. *Hum Mutat*. 2015;36(4):395–402.
10. Yang J, et al. MLPA-based genotype-phenotype analysis in 1053 Chinese patients with DMD/BMD. *BMC Med Genet*. 2013;14:29.
11. Nakamura A, et al. Follow-up of three patients with a large in-frame deletion of exons 45-55 in the Duchenne muscular dystrophy (DMD) gene. *J Clin Neurosci*. 2008;15(7):757–763.
12. Bengtsson NE, et al. Muscle-specific CRISPR/Cas9 dystrophin gene editing ameliorates pathophysiology in a mouse model for Duchenne muscular dystrophy. *Nat Commun*. 2017;8:14454.
13. Li HL, et al. Precise correction of the dystrophin gene in duchenne muscular dystrophy patient induced pluripotent stem cells by TALEN and CRISPR-Cas9. *Stem Cell Reports*. 2015;4(1):143–154.
14. Long C, et al. Postnatal genome editing partially restores dystrophin expression in a mouse model of muscular dystrophy. *Science*. 2016;351(6271):400–403.
15. Long C, McAnally JR, Shelton JM, Mireault AA, Bassel-Duby R, Olson EN. Prevention of muscular dystrophy in mice by CRISPR/Cas9-mediated editing of germline DNA. *Science*. 2014;345(6201):1184–1188.
16. Ousterout DG, Kabadi AM, Thakore PI, Majoros WH, Reddy TE, Gersbach CA. Multiplex CRISPR/Cas9-based genome editing for correction of dystrophin mutations that cause Duchenne muscular dystrophy. *Nat Commun*. 2015;6:6244.
17. Zhang Y, et al. CRISPR-Cpf1 correction of muscular dystrophy mutations in human cardiomyocytes and mice. *Sci Adv*. 2017;3(4):e1602814.
18. Gregorevic P, et al. rAAV6-microdystrophin preserves muscle function and extends lifespan in severely dystrophic mice. *Nat Med*. 2006;12(7):787–789.
19. Sakamoto M, et al. Micro-dystrophin cDNA ameliorates dystrophic phenotypes when introduced into mdx mice as a transgene. *Biochem Biophys Res Commun*. 2002;293(4):1265–1272.
20. Yue Y, et al. Safe and bodywide muscle transduction in young adult Duchenne muscular dystrophy dogs with adeno-associated virus. *Hum Mol Genet*. 2015;24(20):5880–5890.
21. Toh ZY, et al. Deletion of dystrophin in-frame exon 5 leads to a severe phenotype: guidance for exon skipping strategies. *PLoS One*. 2016;11(1):e0145620.
22. Young CS, et al. A single CRISPR-Cas9 deletion strategy that targets the majority of DMD patients restores dystrophin function in hiPSC-derived muscle cells. *Cell Stem Cell*. 2016;18(4):533–540.
23. Tabebordbar M, et al. In vivo gene editing in dystrophic mouse muscle and muscle stem cells. *Science*. 2016;351(6271):407–411.
24. Nelson CE, et al. In vivo genome editing improves muscle function in a mouse model of Duchenne muscular dystrophy. *Science*. 2016;351(6271):403–407.
25. Xu L, et al. CRISPR-mediated genome editing restores dystrophin expression and function in mdx mice. *Mol Ther*. 2016;24(3):564–569.
26. Corrado K, Mills PL, Chamberlain JS. Deletion analysis of the dystrophin-actin binding domain. *FEBS Lett*. 1994;344(2-3):255–260.
27. Henderson DM, Lee A, Ervasti JM. Disease-causing missense mutations in actin binding domain 1 of dystrophin induce thermodynamic instability and protein aggregation. *Proc Natl Acad Sci U S A*. 2010;107(21):9632–9637.
28. Levine BA, Moir AJ, Patchell VB, Perry SV. Binding sites involved in the interaction of actin with the N-terminal region of dystrophin. *FEBS Lett*. 1992;298(1):44–48.
29. Sutherland-Smith AJ, et al. An atomic model for actin binding by the CH domains and spectrin-repeat modules of utrophin and dystrophin. *J Mol Biol*. 2003;329(1):15–33.
30. Wein N, et al. Translation from a DMD exon 5 IRES results in a functional dystrophin isoform that attenuates dystrophinopathy in humans and mice. *Nat Med*. 2014;20(9):992–1000.
31. Lattanzi A, et al. Correction of the Exon 2 duplication in DMD myoblasts by a single CRISPR/Cas9 system. *Mol Ther Nucleic Acids*. 2017;7:11–19.
32. Bish LT, et al. Long-term restoration of cardiac dystrophin expression in golden retriever muscular dystrophy following rAAV6-mediated exon skipping. *Mol Ther*. 2012;20(3):580–589.
33. Echigoya Y, et al. Effects of systemic multiexon skipping with peptide-conjugated morpholinos in the heart of a dog model of Duchenne muscular dystrophy. *Proc Natl Acad Sci U S A*. 2017;114(16):4213–4218.
34. Kaspar RW, et al. Analysis of dystrophin deletion mutations predicts age of cardiomyopathy onset in becker muscular dystrophy. *Circ Cardiovasc Genet*. 2009;2(6):544–551.
35. Novaković I, et al. Proximal dystrophin gene deletions and protein alterations in becker muscular dystrophy. *Ann N Y Acad Sci*. 2005;1048:406–410.
36. Singh SM, Kongari N, Cabello-Villegas J, Mallela KM. Missense mutations in dystrophin that trigger muscular dystrophy decrease protein stability and lead to cross-beta aggregates. *Proc Natl Acad Sci U S A*. 2010;107(34):15069–15074.
37. Heald A, Anderson LV, Bushby KM, Shaw PJ. Becker muscular dystrophy with onset after 60 years. *Neurology*. 1994;44(12):2388–2390.
38. Nakamura A, et al. Deletion of exons 3-9 encompassing a mutational hot spot in the DMD gene presents an asymptomatic phenotype, indicating a target region for multiexon skipping therapy. *J Hum Genet*. 2016;61(7):663–667.

39. Matsa E, Ahrens JH, Wu JC. Human induced pluripotent stem cells as a platform for personalized and precision cardiovascular medicine. *Physiol Rev*. 2016;96(3):1093–1126.
40. Tiburcy M, et al. Defined engineered human myocardium with advanced maturation for applications in heart failure modeling and repair. *Circulation*. 2017;135(19):1832–1847.
41. Talsness DM, Belanto JJ, Ervasti JM. Disease-proportional proteasomal degradation of missense dystrophins. *Proc Natl Acad Sci U S A*. 2015;112(40):12414–12419.
42. Fletcher S, et al. Targeted exon skipping to address "leaky" mutations in the dystrophin gene. *Mol Ther Nucleic Acids*. 2012;1:e48.
43. Winnard AV, Mendell JR, Prior TW, Florence J, Burghes AH. Frameshift deletions of exons 3-7 and revertant fibers in Duchenne muscular dystrophy: mechanisms of dystrophin production. *Am J Hum Genet*. 1995;56(1):158–166.
44. Guan X, et al. Dystrophin-deficient cardiomyocytes derived from human urine: new biologic reagents for drug discovery. *Stem Cell Res*. 2014;12(2):467–480.
45. Lin B, et al. Modeling and study of the mechanism of dilated cardiomyopathy using induced pluripotent stem cells derived from individuals with Duchenne muscular dystrophy. *Dis Model Mech*. 2015;8(5):457–466.
46. Rajdev A, Groh WJ. Arrhythmias in the muscular dystrophies. *Card Electrophysiol Clin*. 2015;7(2):303–308.
47. Yumlu S, et al. Gene editing and clonal isolation of human induced pluripotent stem cells using CRISPR/Cas9. *Methods*. 2017;121-122:29–44.
48. Veres A, et al. Low incidence of off-target mutations in individual CRISPR-Cas9 and TALEN targeted human stem cell clones detected by whole-genome sequencing. *Cell Stem Cell*. 2014;15(1):27–30.
49. Yang L, et al. Targeted and genome-wide sequencing reveal single nucleotide variations impacting specificity of Cas9 in human stem cells. *Nat Commun*. 2014;5:5507.
50. Aartsma-Rus A, Ginjaar IB, Bushby K. The importance of genetic diagnosis for Duchenne muscular dystrophy. *J Med Genet*. 2016;53(3):145–151.
51. Odom GL, Gregorevic P, Allen JM, Chamberlain JS. Gene therapy of mdx mice with large truncated dystrophins generated by recombination using rAAV6. *Mol Ther*. 2011;19(1):36–45.
52. Banks GB, Gregorevic P, Allen JM, Finn EE, Chamberlain JS. Functional capacity of dystrophins carrying deletions in the N-terminal actin-binding domain. *Hum Mol Genet*. 2007;16(17):2105–2113.
53. Acsadi G, et al. Novel mutation in spectrin-like repeat 1 of dystrophin central domain causes protein misfolding and mild Becker muscular dystrophy. *J Biol Chem*. 2012;287(22):18153–18162.
54. Corrado K, et al. Transgenic mdx mice expressing dystrophin with a deletion in the actin-binding domain display a "mild Becker" phenotype. *J Cell Biol*. 1996;134(4):873–884.
55. van Putten M, et al. The effects of low levels of dystrophin on mouse muscle function and pathology. *PLoS One*. 2012;7(2):e31937.
56. Wells DJ, et al. Expression of human full-length and minidystrophin in transgenic mdx mice: implications for gene therapy of Duchenne muscular dystrophy. *Hum Mol Genet*. 1995;4(8):1245–1250.
57. Neri M, et al. Dystrophin levels as low as 30% are sufficient to avoid muscular dystrophy in the human. *Neuromuscul Disord*. 2007;17(11–12):913–918.
58. Young CS, Mokhonova E, Quinonez M, Pyle AD, Spencer MJ. Creation of a novel humanized dystrophic mouse model of duchenne muscular dystrophy and application of a CRISPR/Cas9 gene editing therapy. *J Neuromuscul Dis*. 2017;4(2):139–145.
59. Ran FA, Hsu PD, Wright J, Agarwala V, Scott DA, Zhang F. Genome engineering using the CRISPR-Cas9 system. *Nat Protoc*. 2013;8(11):2281–2308.
60. Burridge PW, et al. Chemically defined generation of human cardiomyocytes. *Nat Methods*. 2014;11(8):855–860.